Lithium sputtering from lithium-coated plasma facing components in the NSTX divertor

CrossMark

F. Scotti [a],[*], V.A. Soukhanovskii [a], J.-W. Ahn [b], R.E. Bell [c], S.P. Gerhardt [c], M.A. Jaworski [c], R. Kaita [c], H.W. Kugel [c], A.G. McLean [a], E.T. Meier [a], M. Podestà [c], A.L. Roquemore [c]

[a] Lawrence Livermore National Laboratory, Livermore, 94551 CA, USA
[b] Oak Ridge National Laboratory, Oak Ridge, 37831 TN, USA
[c] Princeton Plasma Physics Laboratory, Princeton, 08543 NJ, USA

ARTICLE INFO

ABSTRACT

Lithium sputtering yields and gross impurity influxes from lithium-coated graphite and molybdenum plasma facing components (PFCs) have been analyzed for the first time in the National Spherical Torus Experiment (NSTX) divertor during H-mode NBI-heated discharges. Motivated by the beneficial effects of lithium conditioning on discharge performance and reproducibility, evaporative lithium coatings were the routine wall conditioning technique in NSTX. Neutral lithium sputtering yields from solid lithium coatings in NSTX were found to be consistent with values reported from test stand experiments from deuterium-saturated lithium (with sputtering yields $Y_{Li} \sim 0.03-0.07$). Temperature-enhanced lithium sputtering was observed on lithium-coated graphite and molybdenum as a result of PFC heating by both embedded heaters and incident plasma heat flux, leading to $Y_{Li} \sim 0.1-0.2$ for surface temperatures above the lithium melting point.

© 2014 Published by Elsevier B.V.

1. Introduction

In order to satisfy the varied requirements for wall and divertor plasma facing components (PFCs), future fusion devices, such as ITER [1], will use different materials for the PFCs. Material erosion, migration and re-deposition, will lead to a mixed material environment, with properties which could differ from those of the virgin components [2]. Understanding the synergies of different materials in terms of fuel retention, sputtering, and potential for core contamination will be important for designing the PFCs of future machines.

The National Spherical Torus Experiment (NSTX) [3] employed mixed materials for the PFCs, with lithium conditioning via evaporative coatings applied onto graphite and molybdenum [4]. Accumulation of carbon impurities was routinely observed in the core of ELM-free lithium-conditioned discharges in NSTX [5]. Core lithium densities were less than 0.1% of the core electron densities despite the large lithium depositions [6]. The different core impurity accumulation of carbon and lithium was only partially explained by the difference in their core radial transport [5] and motivated a deeper investigation of the sputtering and scrape-off layer (SOL) transport behavior of the two impurities in NSTX. This paper aims at characterizing lithium sputtering yield and gross divertor influxes in NSTX.

2. Experimental setup and method

In NSTX, starting from the 2010 experimental campaign, several materials were employed for the lower divertor PFCs. Two rows of ATJ graphite tiles formed the inboard divertor ($R = 28-57$ cm) while the outer divertor was composed of a row of graphite bull-nose tiles (BN, $R = 61-65$ cm), and the liquid lithium divertor (LLD, $R = 65-84$ cm). The LLD consisted of four toroidal segments (each about 80° toroidally) of porous molybdenum ($\sim$170 μm thick with 0.1 μm characteristic porosity scale length) plasma sprayed on a stainless steel liner (0.25 mm thick) brazed to a copper plate (2.2 cm thick) with embedded heaters and thermocouples [7]. The four LLD plates were separated from each other by four diagnostic graphite tiles.

Lithium coatings were applied on the lower divertor by two evaporators toroidally separated by 150°. Chemical reactions with deuterium and vacuum impurities, erosion, evaporation and inter-calation in graphite limited the lifetime of active lithium coatings [8], so lithium evaporations were performed before every discharge. Typically, 100–400 mg of lithium were evaporated between discharges. This evaporation corresponds to a nominal lithium coating peak thickness of 20–80 nm or areal densities of

$1–4 \times 10^{21}$ atoms/m^2, with a toroidal asymmetry in deposition up to a factor of 3 [4]. This paper presents data from the 2010 experimental campaign. Lower single null, NBI-heated, H-mode discharges with lithium conditioning are analyzed. The outer strike point (OSP) was in the outer divertor ($R \geqslant 61$ cm) and in attached conditions. A large lithium evaporation (16 g) was carried out before the beginning of the experimental campaign, without any boronization. By the end of the 2010 campaign, about 845 g of lithium were evaporated in the vacuum vessel, which corresponds to lithium areal densities up to 8×10^{24} atoms/m^2 on the divertor PFCs.

Impurity influxes from the PFCs were determined from the line-integrated brightness measured by divertor imaging cameras [9] and interpreted via the ionizations per photon method (S/XB) [10], using coefficients from the ADAS database [11]. Two-dimensional cameras (filtered with narrow bandpass filters) provided full coverage (radial and toroidal) of the lower divertor with 1-cm resolution [9]. The neutral lithium line at 670.8 nm (Li I) and singly ionized line at 548.5 nm (Li II) were used for the determination of lithium line-integrated brightness. Incident ion fluxes were measured by the Langmuir probes in the high density Langmuir probe (HDLP) array [12]. The HDLP array was located in one of the diagnostic tiles in the outer divertor and was equipped with 4 single (swept at 1 kHz) and 5 triple (digitized at 250 kHz) probes at radii between 63 and 71 cm. Electron temperatures (T_e) and electron densities (n_e) from the HDLP array were used to determine S/XB coefficients. Uncertainties in T_e and J_{SAT} obtained from the fit of the classical I–V curve to the probe characteristic were propagated to determine the error in n_e and in the S/XB coefficients. S/XB coefficients were applied to line integrated brightness to infer impurity influxes, and impurity sputtering yields were then determined from the ratio of the impurity influxes and the incident ion fluxes. For the comparison with tabulated values of sputtering yields, ion temperatures T_i (not measured for the NSTX divertor) were taken to be equal to T_e, leading to an incident ion energy of $5 \times T_e$, while the angle of incidence of the ions was assumed to be 45°. The neutral fraction of 1/3 was assumed for the comparison of measured neutral lithium sputtering yields with tabulated values of total lithium sputtering yields [13].

3. Results and discussion

Heaters embedded in the PFCs enabled the testing of the response of lithium influx and sputtering yield on molybdenum substrates as a function of the surface temperature (T_{surf}). In this section, two discharges are compared, both of which were performed after a large lithium evaporation of 200 g (and a campaign-integrated lithium evaporation of 530 g), equivalent to a peak nominal coating thickness of ~40 μm. This thickness was larger than the LLD porosity and greater than the typical surface roughness of graphite in NSTX [14]. These discharges had similar plasma parameters ($P_{NBI} = 3$ MW, $I_P = 900$ kA, $\delta r_{sep} \sim -2$ cm) and the OSP in the lower outer divertor with peak divertor incident fluxes $\sim 1 \times 10^{23}$ ions/m^2/s. Divertor T_e and n_e values as measured by the Langmuir probes were in the range of 5–25 eV and $1–10 \times 10^{19}$ m^{-3}. In the first discharge (139598), three LLD plates were heated to ~220 °C while one was left unheated due to a failure of the embedded heaters. In the second discharge (139769), all four LLD plates were left unheated and were below the lithium melting point ($T_m = 180.5$ °C). The first discharge was performed right after the large lithium evaporation while the second was carried out 130 discharges later (with an accumulated plasma exposure of ~83 s and an integrated ion fluence of $\sim 2 \times 10^{24}$ ions/m^2 at the 70.5 cm probe), without any pre-discharge ("fresh") lithium evaporation. The integrated ion fluence was comparable to the

lithium areal density from the 200 g evaporation, so the lithium surface could be expected to have been partially saturated with deuterium.

The higher T_{surf} on the heated LLD plates led to the local enhancement of lithium influxes with respect to unheated LLD plates and graphite. In Fig. 1(a) and (b), contour plots of lower divertor Li I emission are plotted for the two discharges in consideration (139598 and 139769, respectively) at $t = 0.5$ s as a function of the divertor radius R and toroidal angle ϕ. In Fig. 1(a), higher lithium emission was observed on the three heated LLD segments ($R = 65–84$ cm, $\phi = 10°$, 100°, 280°), while emission on the graphite diagnostic tiles ($R = 65–84$ cm, $\phi = 55°$, 145°, 225°) was comparable to the emission on the unheated LLD plate ($\phi = 190°$). In contrast, in the discharge where all the LLD plates were unheated (Fig. 1(b)) no clear difference was observed between the various LLD segments and the graphite tiles. The relative enhancement in lithium influxes can be seen more clearly from the ratio of the brightness at a given radial location in the two discharges, plotted in Fig. 1(c) as
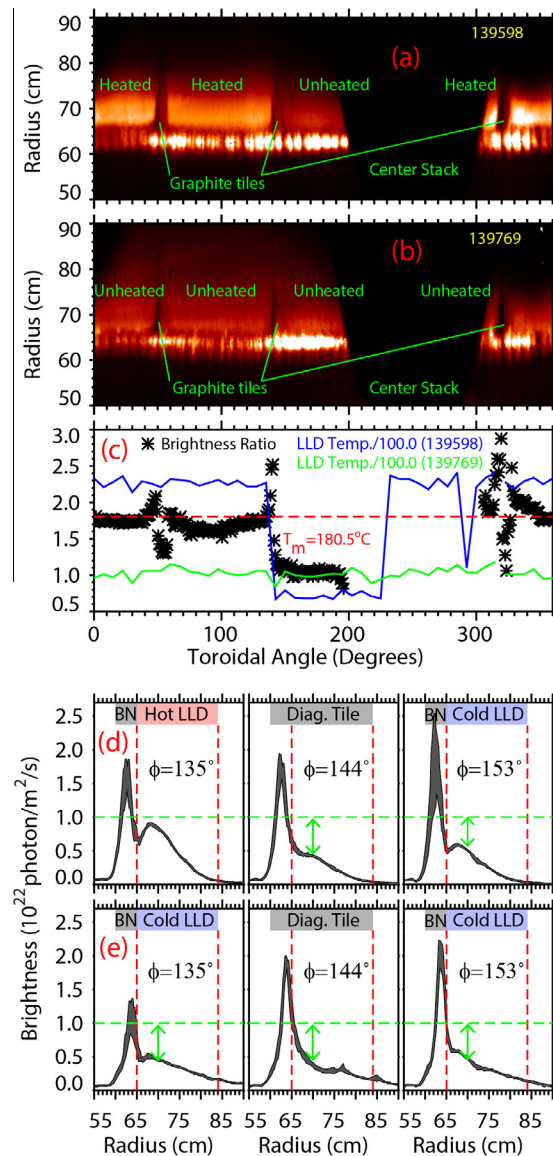
Fig. 1. Li I emission in discharge 139598 (a) and 139769 (b); ratio of the line integrated brightness as a function of ϕ at $R = 70$ cm (black asterisks) and bulk LLD temperature for discharge 139598 (blue) and 139769 (green) (c); and radial profiles of Li I brightness in discharge 139598 (d) and 139769 (e) at different toroidal locations. (For interpretation of the references to color in this figure legend, the reader is referred to the web version of this article.)

a function of ϕ. While no difference was observed on graphite and on the LLD plate which was unheated in both discharges and remained below the lithium melting point (T_{surf} up to 160 °C at 71 cm), an enhancement of a factor up to 1.5–2 was seen over the heated plates. In the same plot, the bulk temperatures of the copper plates are plotted for the two discharges as measured by the embedded thermocouples. This enhancement is qualitatively consistent with the temperature-enhanced ("thermal") sputtering observed on test stands (PISCES [15,16] and IIAX [13]), which was attributed to the dependence of the effective lithium surface binding energy on T_{surf}. It must be noted that, while plasma parameters are assumed to be toroidally uniform, any local increase in n_e due to the higher lithium influxes on the heated plates would further augment this enhancement due the dependence of the Li I S/XB coefficient on n_e and its insensitivity to T_e.

No clear difference in neutral lithium emission could be observed between unheated molybdenum and graphite substrates. In Fig. 1(d) and (e), the gray bands show the radial profiles of lithium line-integrated brightness at three different ϕ (135°, 144°, 153°, locations corresponding to hot LLD, diagnostic tile and cold LLD in discharge 139598, respectively) within a 3° range toroidally for discharges 139598 and 139769. Dashed vertical lines indicate the location of the LLD (65–84 cm). From these figures, comparable lithium emission is observed in both discharges on cold LLD and on the diagnostic tile (both of which are reduced if compared to the hot LLD case in Fig. 1(d) – left). While a reduction in lithium sputtering was measured on lithiated graphite in IIAX [17] and was attributed to the formation of ionic bonds between carbon and lithium, the NSTX result can be understood as due to the macroscopically thick lithium coatings, which reduce the role of the substrate in determining the surface sputtering.

Sputtering yields determined for solid and liquid lithium coatings in NSTX were consistent with expectations from physical and "thermal" sputtering from deuterium-saturated lithium. The measured local lithium influxes are $\sim 1 \times 10^{21}$–1×10^{22} atoms/m^2/s, several orders of magnitude larger than the evaporative fluxes expected at $T_{surf} \sim 200$–300 °C (up to 1×10^{19} atoms/m^2/s). For these T_{surf}, measured lithium influxes are therefore due to lithium physical and "thermal" sputtering and can be used for the determination of the effective sputtering yield Y_{Li}. In Fig. 2(a) and (b), temporal waveforms of lithium influxes (a) at one of the triple probe locations ($R = 71$ cm) and the inferred neutral lithium sputtering yields (b) are plotted as a function of time as measured on graphite (diagnostic tile – black) and molybdenum (heated LLD plate – red and unheated LLD plate – blue). While the local influxes at the probe location vary by as much as an order of magnitude during the discharge due to the drift of the OSP over time, the inferred local sputtering yield was constant as a result of the weak dependence of Y_{Li} on the incident energies (estimated to be between 60 and 125 eV at this location) above the sputtering threshold and the relatively unchanged T_{surf}. The measured values of $Y_{Li} \sim 3$–7% are consistent with estimates from bca (binary collision approximation) codes (SRIM–TRIM [18]) and values reported from test stand experiments on deuterium-saturated lithium surfaces. An enhancement of the sputtering yield up to a factor of 2 was observed as a result of the heating of the PFCs to 250 °C (red vs. blue trace). The local enhancement in sputtering yield is also seen in the radial profiles of lithium sputtering yields as a function of $R - R_{OSP}$ shown in Fig. 2(c), where yields calculated at two triple probe locations ($R = 63, 71$ cm) have been plotted during a 100 ms sweep of the OSP location. The sputtering yields calculated on the bullnose graphite tile ($R = 63$ cm) do not systematically vary at the three different toroidal locations, indicating that the asymmetry in lithium emission at 71 cm is not due to intrinsic toroidal asymmetries in incident particle fluxes.
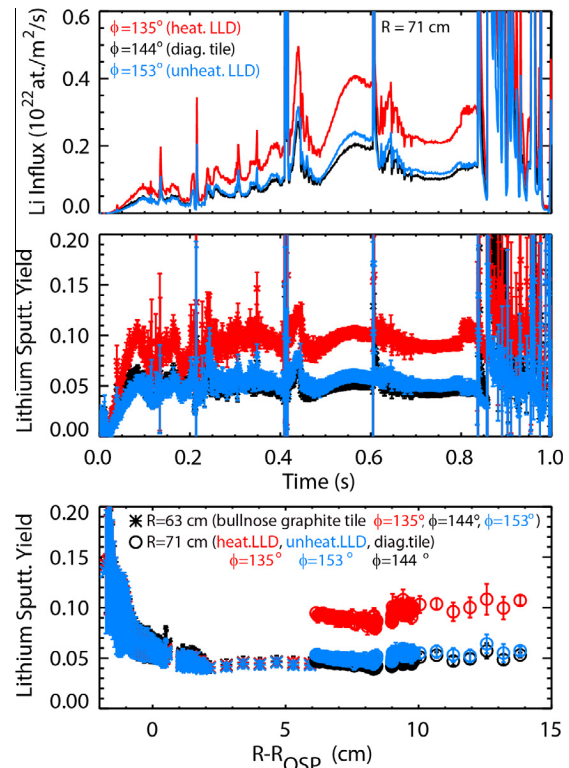
Fig. 2. Neutral lithium influxes and sputtering yield from the probe at $R = 71$ cm as a function of time (a and b) at three different toroidal locations: graphite tile (black), heated LLD (red) and unheated LLD (blue); neutral lithium sputtering yield (c) at the same toroidal locations as a function of $R - R_{OSP}$ from the probe at $R = 71$ cm (circles) and at $R = 63$ cm (asterisks). (For interpretation of the references to color in this figure legend, the reader is referred to the web version of this article.)

The response of the lithium sputtering yield to changes in T_{surf} (as a result of heating due to the local incident plasma heat flux), has also been analyzed on graphite substrates, showing reasonable agreement with expectations from deuterium-saturated liquid lithium. In Fig. 3, the lithium sputtering yield as measured in discharge 139769 at several probe locations ($R = 63, 64, 67$ cm) in the vicinity of the OSP is plotted as a function of the T_{surf} measured by the two-color IR camera [19]. In this plot, error bars include also the variability of the lithium influxes and T_{surf} over the toroidal angle (4°) used for the averaging of the IR and spectroscopic
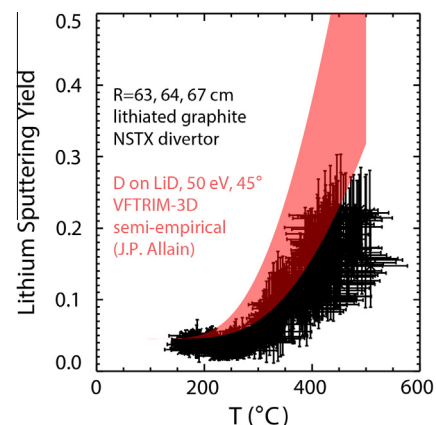
Fig. 3. Neutral lithium sputtering yield as a function of surface temperature from lithium-coated graphite tiles.

measurements. To minimize the effect of leading edges on the lithium sputtering estimates (evident from the contour plots in Fig. 1(a) and (b) and from IR thermography), toroidal averaging was performed on the central part of the graphite tile with the largest toroidal extent (the diagnostic graphite tile). Measurements of the lithium sputtering yield over a range of T_{surf} between 50 °C and 450 °C were obtained, with Y_{Li} up to 0.25. In Fig. 3, neutral lithium sputtering yield from a VFTRIM-3D semi-empirical model by J.P. Allain based on IIAX results [20] for deuterium incident at 45° and 50 eV on deuterium-saturated lithium is also overlaid, showing reasonable agreement with the NSTX data (albeit with slightly higher values).

While the effective lithium sputtering yield measured on thick lithium coatings in NSTX was consistent with expectations from physical and "thermal" sputtering due to deuterium incident on deuterium-saturated lithium, the lithium surface in NSTX can be contaminated with carbon and oxygen [21]. Furthermore, the effect of lithium sputtering due to impurities (self-sputtering and carbon) was not included. Due to the relatively similar Y_{Li} due to incident deuterium (Y_{Li-D}), carbon (Y_{Li-C}) and lithium (Y_{Li-Li}) ions (within a factor of 2 according to SRIM–TRIM) at typical NSTX divertor incident energies ($\sim$50–100 eV), the inclusion of sputtering due to impurities is not expected to significantly affect the results. While the carbon contribution is negligible, the inclusion of lithium self-sputtering could lead to a deviation of Y_{Li-D} from the measured effective yield, Y_{Li}. However, for the highest Y_{Li} case in this work ($\sim$0.2), and assuming 100% re-deposition, the measured effective Y_{Li} would overestimate Y_{Li-D} by only 15%, thus not affecting the conclusions. Further complicating factors in the interpretation of these results are the possibly different sputtering behavior of re-deposited lithium layers with respect to freshly evaporated coatings (e.g., as observed for beryllium in PISCES [2]) and the possible contribution of lithium droplet ejection to the measured lithium influxes.

Despite the large gross lithium influxes, re-deposition effects are expected to play an important role in regulating both the lifetime of lithium coatings and the core contamination of lithium ions in NSTX. Even with more typical lithium "doses" ($\sim$ few 100s mg), sputtering yields comparable to those presented in this section have been measured, without any indication of decreasing lithium influxes over the course of 1 s NSTX discharges [22]. Since the measured gross Y_{Li} would lead to the complete erosion of pre-applied coatings within a few 100s ms, this is suggestive of the importance of re-deposition effects, but the relative role of accumulated vs. "fresh" lithium coatings on the lithium influxes still needs to be characterized. A large prompt re-deposition fraction (resulting from the ionization mean free path being much shorter than the ion gyro-radius) was predicted by kinetic simulations with WBC-REDEP [20], and is consistent with the measurements of singly ionized lithium influxes, which are typically $\sim$1 or 2 orders of magnitude lower than the neutral lithium influxes at the OSP. Integrating the OSP neutral lithium influxes, gross lithium influxes in NSTX

H-modes are estimated at $\sim 1-5 \times 10^{21}$ atoms/s. Comparing the gross influxes with the lithium core particle inventories ($\sim$ few 10^{17} ions) as measured by charge exchange recombination spectroscopy [6], very low penetration factors are determined ($\sim 10^{-4}-10^{-3}$). This is much less than what inferred for carbon ($\sim 10^{-1}$) and can be associated with the strong divertor retention of lithium as a result of both prompt re-deposition and the effect of classical parallel SOL forces, as evident from UEDGE simulations [22].

4. Conclusions

Lithium sputtering yields and gross impurity influxes from lithium-coated divertor PFCs have been analyzed for the first time in NSTX H-mode NBI-heated discharges. Neutral lithium sputtering yields from lithium coatings were found to be consistent with values reported from test stand experiments from solid and liquid deuterium-saturated lithium, with Y_{Li} up to $\sim$0.2. Temperature-enhanced lithium sputtering was observed from lithium coatings on both graphite and molybdenum substrates. These measurements contribute to the development of the physics basis for the use of lithium coatings as a PFC. Studying the behavior of lithium coatings in ITER-relevant divertor heat and particle fluxes in the NSTX-Upgrade [23] will further clarify the potential for the application of solid/liquid lithium PFCs in future fusion reactors.

References

[1] ITER Physics Expert Group on divertor, Nucl. Fusion 39 (1999) 2391.
[2] R. Doerner et al., Nucl. Fusion 52 (2012) 103003.
[3] M. Ono et al., Nucl. Fusion 40 (2000) 557.
[4] H. Kugel et al., Phys. Plasmas 15 (2008) 056118.
[5] F. Scotti et al., Nucl. Fusion 53 (2013) 083001.
[6] M. Podestà et al., Nucl. Fusion 52 (2012) 033008.
[7] H. Kugel et al., Fusion Eng. Des. 84 (2009) 1125–1129.
[8] W. Wampler et al., J. Nucl. Mater. 390–391 (2009) 1009–1012.
[9] F. Scotti et al., Rev. Sci. Instrum. 83 (2012) 10E532.
[10] K. Behringer et al., Plasma Phys. Control. Fusion 31 (1989) 2059.
[11] H.P. Summers, The ADAS User Manual, 2004 <http://www.adas.ac.uk>.
[12] J. Kallman et al., Rev. Sci. Instrum. 81 (2010) 10E117.
[13] J. Allain et al., Phys. Rev. B 76 (2007) 205434.
[14] C. Taylor et al., J. Appl. Phys. 114 (2013) 223301.
[15] R. Doerner et al., J. Nucl. Mater. 290–293 (2001) 166–172.
[16] R. Doerner et al., J. Nucl. Mater. 313–316 (2003) 383–387.
[17] M. Racic et al., J. Nucl. Mater. 390–391 (2009) 1043–1047.
[18] <http://www.srim.org/>.
[19] A. Mclean et al., Rev. Sci. Instrum. 83 (2012) 053706.
[20] J. Allain et al., Nucl. Fusion 51 (2011) 023002.
[21] C. Skinner et al., J. Nucl. Mater. 438 (2013) S647–S650.
[22] F. Scotti, Ph.D. Thesis, Princeton University, 2014.
[23] J.M. Menard et al., Nucl. Fusion 52 (2012) 083015.